Biomech Model Mechanobiol (2012) 11:983–993
DOI 10.1007/s10237-011-0367-2

ORIGINAL PAPER

Mechanical behaviour of in-situ chondrocytes subjected to different loading rates: a finite element study

E. K. Moo · W. Herzog · S. K. Han · N. A. Abu Osman · B. Pingguan-Murphy · S. Federico

Received: 24 June 2011 / Accepted: 8 December 2011 / Published online: 11 January 2012

Abstract Experimental findings indicate that in-situ chondrocytes die readily following impact loading, but remain essentially unaffected at low (non-impact) strain rates. This study was aimed at identifying possible causes for cell death in impact loading by quantifying chondrocyte mechanics when cartilage was subjected to a 5% nominal tissue strain at different strain rates. Multi-scale modelling techniques were used to simulate cartilage tissue and the corresponding chondrocytes residing in the tissue. Chondrocytes were modelled by accounting for the cell membrane, pericellular matrix and pericellular capsule. The results suggest that cell deformations, cell fluid pressures and fluid flow velocity through cells are highest at the highest (impact) strain rate, but they do not reach damaging levels. Tangential strain rates of the cell membrane were highest at the highest strain rate and were observed primarily in superficial tissue cells. Since cell death following impact loading occurs primarily in superficial zone cells, we speculate that cell death in impact loading is caused by the high tangential strain rates in the membrane of superficial zone cells causing membrane rupture and loss of cell content and integrity.

Keywords Finite element modelling · Impact loading · Chondrocyte mechanics · Cell membrane damage · Osteoarthritis · Cartilage mechano-biology

E. K. Moo (✉) · N. A. Abu Osman · B. Pingguan-Murphy
Department of Biomedical Engineering, Faculty of Engineering, University of Malaya, Kuala Lumpur, Malaysia
e-mail: ekmoo@hotmail.my

W. Herzog · S. K. Han
Human Performance Laboratory, Faculty of Kinesiology, The University of Calgary, Calgary, Canada

W. Herzog
e-mail: walter@kin.ucalgary.ca

W. Herzog · S. Federico
Department of Mechanical and Manufacturing Engineering, Schulich School of Engineering, The University of Calgary, Calgary, Canada

S. Federico
e-mail: salvatore.federico@ucalgary.ca

1 Introduction

Osteoarthritis (OA) is a degenerative, chronic joint disease, ultimately leading to complete erosion of the articular cartilage (Brandt et al. 1986). Onset of secondary OA has been associated with joint trauma often involving impact loading that causes chondrocyte (cartilage cell) death (Blanco et al. 1998; Simon et al. 1976) and thus a reduced capacity for cartilage to adapt and repair (Mankin 1963).

There is an abundance of studies aimed at investigating the effects of joint impact loading on cartilage damage and chondrocyte death (Ewers et al. 2001; Repo and Finlay 1977; Milentijevic et al. 2003; Milentijevic and Torzilli 2005). Some of these have suggested that chondrocyte death depends greatly on the rate and magnitude of strain (Ewers et al. 2001; Repo and Finlay 1977; Kurz et al. 2001; Quinn et al. 2001) and that cell death for impact loads occurs primarily in the superficial zone of cartilage. However, it is not clearly established why high strain rates cause chondrocyte death, while equivalent magnitudes of strain applied slowly do not. Furthermore, although cell deformations can be measured in the intact joint for slow load applications (Abusara et al. 2011), such measurements will not be possible in the near future for impact loading where a temporal resolution of 10^{-4} s is required for proper analysis.

Therefore, the purpose of this study was to investigate the effects of strain rates on in-situ chondrocyte mechanics using

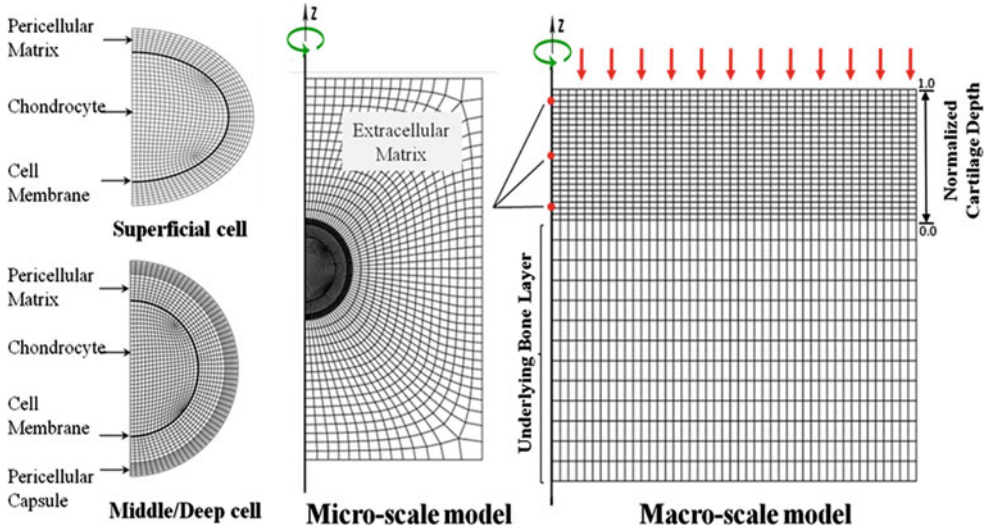

Fig. 1 Articular cartilage tissue (macro-scale) and chondrons (micro-scale) axisymmetric mesh models; Macro-scale model: The bone layer is assumed 2 mm thick and the cartilage is modelled as 1 mm thick. The normalized cartilage tissue depth, ξ, runs vertically from the tidemark (cartilage–bone interface) to the articular surface. *The red arrows* represent the direction of the applied nominal strain on the articular surface. The time-varying responses at depth $\xi = 0.1$ (deep zone), $\xi = 0.5$ (middle zone), $\xi = 0.9$ (superficial zone) are applied as boundary conditions for the cell model located in the deep, middle and superficial zone, respectively; Micro-scale model: It consists of chondrons embedded in an extracellular matrix (ECM). Chondrons are composed of chondrocytes surrounded by a cell membrane, pericellular matrix and a pericellular capsule. Superficial zone cells lack the pericellular capsule (Poole et al. 1987)

a computational approach based on Finite Element analysis. Changes in the cell mechanics were studied as a function of strain rate. We propose that the differences in cell mechanics at the different strain rates might point to the reason for cells dying at high but not at low strain rates.

2 Methodology

In order to model the mechanical behaviour of chondrocytes, we use a two-scale modelling approach for the cartilage tissue and the embedded cells as described in the literature (Guilak and Mow 1992; Mow and Guilak 1993; Wu and Herzog 2000; Han et al. 2007). The two-scale model was comprised of a macro-scale model to represent the cartilage tissue and a micro-scale model to represent individual cells. An axisymmetric model was used throughout the study to save computational cost.

2.1 Macro-scale model

An osteochondral sample was modelled as a layer of articular cartilage "mounted" on a layer of subchondral bone (Fig. 1). A normalized cartilage depth, ξ, was defined vertically from the tidemark (cartilage–bone interface, $\xi = 0$) to the articular surface ($\xi = 1$). Cartilage was assumed to be a biphasic material consisting of a solid phase and a fluid phase. The solid phase was considered as hyperelastic, and the elastic strain energy potential was assumed to be isotropic. Holmes and Mow's elastic potential (Holmes and Mow 1990) was chosen to represent the extracellular matrix (ECM),

$$W_m = \alpha_0 \frac{\exp[\alpha_1(I_1 - 3) + \alpha_2(I_2 - 3)]}{(I_3)^{\beta}}, \tag{1}$$

where $I_1(\boldsymbol{C})$, $I_2(\boldsymbol{C})$, $I_3(\boldsymbol{C})$ are the three principal invariants of the right Cauchy–Green deformation tensor of the solid phase, $\boldsymbol{C} = \boldsymbol{F}^T\boldsymbol{F}$ ($\boldsymbol{F}$ is the deformation gradient tensor of the solid phase); α_0 is a constant with physical dimensions of energy per unit volume; α_1, α_2, $\beta = \alpha_1 + 2\alpha_2$ are dimensionless material constants (Holmes and Mow 1990), related to Lamé's coefficients (λ, μ), Young's modulus (E) and the Poisson's ratio (ν) of the linear elastic theory (Holmes and Mow 1990; Wu and Herzog 2000) by

$$\frac{E\,\nu}{(1+\nu)(1-2\nu)} = \lambda = 4\alpha_2\,\alpha_0, \tag{2}$$

$$\frac{E}{2(1+\nu)} = \mu = 2(\alpha_1 + \alpha_2)\alpha_0. \tag{3}$$

For the biphasic mixture, the Cauchy stress is given by

$$\boldsymbol{\sigma} = -p\,\boldsymbol{i} + \boldsymbol{\sigma}^c, \tag{4}$$

where p is the pore pressure, $\boldsymbol{i}$ is the identity tensor, and $\boldsymbol{\sigma}^c$ is the constitutive contribution of the solid phase to the Cauchy stress. For the case of a hyperelastic solid phase, this contribution is typically denoted $\boldsymbol{\sigma}^E$ (elastic).

The elastic Cauchy stress tensor, $\boldsymbol{\sigma}^E$, and the spatial elasticity tensor, $\mathbb{c}$, are related to the elastic strain energy potential by the inverse Piola transformations

$$\sigma_{ij}^E = 2J^{-1}F_{iI}\frac{\partial W}{\partial C_{IJ}}F_{jJ}, \tag{5}$$

$$\mathrm{c}_{ijkl} = 4J^{-1}F_{iI}F_{jJ}\frac{\partial^2 W}{\partial C_{IJ}\partial C_{KL}}F_{kK}F_{lL}, \tag{6}$$

where $J = \det \boldsymbol{F}$ is the volume ratio.

The fluid flow within the tissue was assumed to obey Darcy's law,

$$\boldsymbol{w} = -k \operatorname{grad} p, \tag{7}$$

where $\boldsymbol{w}$ is the filtration velocity, k is the (isotropic) permeability, and p is the pore fluid pressure. The isotropic permeability, k, was described as strain dependent, with the expression of Holmes and Mow (1990) in the form given by Wu and Herzog (2000), as a function of the void ratio, e, which is the ratio of the fluid volumetric fraction ϕ_f to the solid volumetric fraction ϕ_s,

$$k = k_0\left(\frac{e}{e_0}\right)^{\kappa}\exp\left\{\frac{M}{2}\left[\left(\frac{1+e}{1+e_0}\right)^2 - 1\right]\right\}, \tag{8}$$

where κ and M are non-dimensional material parameters that need to be determined experimentally (Holmes and Mow 1990), k_0 is the initial permeability, and e_0 is the initial void ratio.

All mechanical properties of articular cartilage were assumed to be depth dependent and were described as a function of the normalized cartilage tissue depth, running from the bone–cartilage interface, $\xi = 0$, to the articular surface, $\xi = 1$ (Federico et al. 2005; Han et al. 2007). The subchondral bone, modelled as biphasic and linearly elastic, was assumed to be homogeneous.

The aggregate elastic modulus, H_A, which is related to the Young's Modulus, E, and the Poisson's ratio, ν, by

$$E = \frac{(1-2\nu)(1+\nu)}{(1-\nu)}H_A. \tag{9}$$

and the Poisson's ratio, ν, were extrapolated from the depth-dependent measurements made by Schinagl et al. (1997) and Wang et al. (2003), respectively, and were represented as a function of tissue depth, ξ (H_A expressed in MPa):

$$\begin{aligned} H_A = {} & -89.0965\,\xi^9 + 1387.28\,\xi^8 - 4789.81\,\xi^7 \\ & + 7334.81\,\xi^6 - 5791\,\xi^5 - 2348.86\,\xi^4 \\ & - 412.918\,\xi^3 + 13.0337\,\xi^2 - 3.58188\,\xi \\ & + 2.49998, \end{aligned} \tag{10}$$

$$\nu = -0.3517\,\xi + 0.3972. \tag{11}$$

Note that the experiments performed by Wang et al. (2003) were aimed at evaluating the anisotropic properties of articular cartilage, which we averaged to obtain the Poisson's ratio as $\frac{1}{2}(\nu_{31} + \nu_{32})$, where the index 3 indicates the axial direction.

Table 1 Material properties used in the macro-scale model (Maroudas and Bullough 1968; Wang et al. 2003; Schinagl et al. 1997)

	Material properties—macroscale			
	E (MPa)	ν	k_0 (10^{-15}m^4/Ns)	e_0
Cartilage (matrix)	Eq. (9)	Eq. (11)	Eq. (12)	4.200
Subchondral bone	2.0×10^3	0.20	1.0×10^{-5}	0.176

Note that the values for permeability and void ratio are for the undeformed cartilage; permeability and void ratio were assumed constant for bone

The polynomial function that describes the dependence of the initial permeability, k_0, on cartilage tissue depth was extrapolated from published experimental data (Maroudas and Bullough 1968) and was expressed in units of 10^{-15}m^4/Ns

$$\begin{aligned} k_0 = {} & 8.241\,\xi^5 - 19.24\,\xi^4 + 13.95\,\xi^3 \\ & - 3.351\,\xi^2 + 0.4880\,\xi + 0.1390. \end{aligned} \tag{12}$$

The osteochondral sample was assumed to have a radius of 3 mm and to be comprised of a 1-mm-thick cartilage tissue layer "mounted" on a 2-mm-thick layer of bone.

The remaining mechanical properties of cartilage and bone are reported in Table 1.

2.2 Micro-scale model

The micro-scale model consists of biphasic chondrons, i.e., chondrocytes with their surrounding pericellular matrix (PCM) and pericellular capsule (PC) (Poole et al. 1987), embedded in the cylindrical extracellular matrix (ECM). Cell, PCM, PC and ECM were assumed to be perfectly bonded (Guilak and Mow 2000).

The material properties of the ECM were assumed to be depth-dependent, non-linear, isotropic and homogeneous and modelled with the Holmes–Mow elastic strain energy potential (Holmes and Mow 1990). The dimensions of the cylindrical ECM were designed to take into account the aspect ratio and volumetric fraction of the embedded chondrocytes at the different depths (Han et al. 2007). The aspect ratio of the ECM cylinder was assumed to be the same as its corresponding chondrocyte (Han et al. 2007), that is,

$$\frac{Y(\xi)}{R(\xi)} = \alpha_c(\xi) = \frac{a_c(\xi)}{b_c(\xi)}, \tag{13}$$

where Y and R are the semi-height and radius of the cylindrical ECM, respectively; a_c is the semi-axis in the direction of the axis of symmetry, and b_c is the semi-axis in the transverse plane. The aspect ratio of a chondrocyte is defined as $\alpha_c = a_c/b_c$.

The ratio of the volumes of the cell and the embedding cylinder was assumed to be equal to the cell volumetric fraction,

$$\frac{V_{cell}(\xi)}{V_{ECM}(\xi)} = \phi_c(\xi) \tag{14}$$

where $\phi_c(\xi)$ is the cell volumetric fraction at the normalized depth ξ.

The initial diameter of the chondrocytes in the middle/deep zone of cartilage tissue was assumed to be 10 μm (Guilak et al. 1995). The aspect ratio, α_c, and the volumetric fraction, ϕ_c, of the cells were used to determine the dimensions of chondrocytes in different layers of cartilage tissue. Both the aspect ratio (Eq. 15) and volumetric fraction (Eq. 16) of the chondrocytes were depth dependent and were based on interpolated polynomials from Han et al. (2007) and the experimental data from Guilak et al. (1995).

$$\alpha_c = \begin{cases} 1 & ;\xi \in [0.0, 0.7], \\ -7.407\xi^2 + 10.37\xi - 2.629 & ;\xi \in [0.7, 1.0]. \end{cases} \tag{15}$$

$$\phi_c = \begin{cases} 0.025 & ;\xi \in [0.0, 0.3], \\ 0.093\xi^2 - 0.056\xi + 0.033 & ;\xi \in [0.3, 0.7], \\ 1.45\xi^2 - 1.955\xi + 0.698 & ;\xi \in [0.7, 1.0]. \end{cases} \tag{16}$$

Chondrocytes were modelled as revolution ellipsoids (spheroids) and were assumed to be biphasic continua (Han et al. 2007; Guilak and Mow 2000). Chondrocytes at different depths exhibit different mechanical properties: superficial zone cells are stiffer than middle/deep zone cells (Shieh and Athanasiou 2006). The solid phase of chondrocytes was assumed to be isotropic, homogenous and linear. The depth-dependent geometry and permeability of chondrocytes were obtained from previous studies (Trickey et al. 2000; Han et al. 2007).

Chondrocytes in the superficial zone lack the PC (Poole et al. 1987) and were, therefore, modelled as being surrounded by the pericellular matrix (PCM) only. The PCM layer in the superficial zone was assumed to be 1.5 μm thick and biphasic. The solid phase of the PCM layer (Alexopoulos et al. 2005a) was assumed to be non-linear, isotropic and homogeneous (Poole et al. 1987).

The thickness of the PCM surrounding the cells in the middle and deep zones was assumed to be 2.0 μm. Middle and deep zone cells are also surrounded by the PC, which was modelled as a biphasic, homogeneous but linear transversely isotropic composite with thickness of 1.0 μm (Han et al. 2011; Federico et al. 2004, 2005).

The permeability of the cells, PCMs and PCs was assumed to be strain dependent (Eq. 8) (Wu and Herzog 2000). The initial permeability, k_0, and initial void ratio, e_0 of the PCM and PC were taken from previous studies (Wu and Herzog 2000; Alexopoulos et al. 2005b).

Chondrocytes are also surrounded by a cell membrane. The cell membrane was modelled as a biphasic 0.1 μm thick layer with a permeability of about 6 orders of magnitude smaller than the permeability of the cell (Ateshian et al. 2007).

The material properties used in the micro-scale model are summarized in Table 2.

Table 2 Material properties used in the micro-scale model (Shieh and Athanasiou 2006; Alexopoulos et al. 2005a,b; Ateshian et al. 2007; Han et al. 2007; Wu and Herzog 2000; Trickey et al. 2000)

	Material properties—micro-scale			
	E (kPa)	ν	k_0 (10^{-15}m^4/Ns)	e_0
Cell (superficial zone)	1.59	0.34	4.200×10^0	4.88
Cell (middle/deep zone)	0.69	0.34	4.200×10^0	4.88
PCM	40	0.04	4.000×10^{-2}	4.00
PC	200	0.05	1.079×10^0	4.00
Cell membrane	40	0.34	3.000×10^{-6}	3.00

2.3 Numerical implementation procedures

The commercial Finite Element software ABAQUS v6.10 was used to implement the model. Quadratic pore pressure elements were used to represent the biphasic nature of the cartilage tissue and chondrocytes. Transient consolidation theory was applied to compute the transient response of the tissue and cell models. A user-defined material (UMAT) was introduced to describe the Holmes–Mow elastic potential. A confined compression test was performed on the tissue model by constraining the lateral surface of the tissue from radial displacement and fixing the subchondral bone at its bottommost boundary. The articular surface of the tissue (macro-scale) model was then subjected to a nominal strain of 5% using four strain rates (0.167%/s, 5%/s, 50%/s, 500%/s) (Fig. 2). The pore pressure was imposed to be zero at the

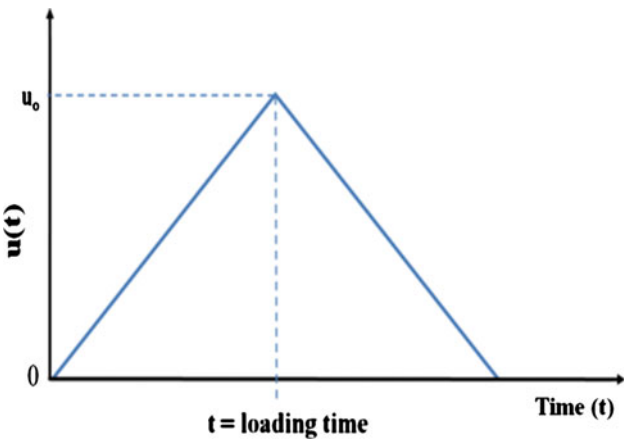

Fig. 2 Load pattern applied to the tissue level model. A nominal strain of 5% was applied to the articular surface at four different strain rates: 0.167%/s, 5%/s, 50%/s, 500%/s. In the graph, $u(t)$ is the nominal strain applied as a function of time, while u_o is the peak nominal strain applied

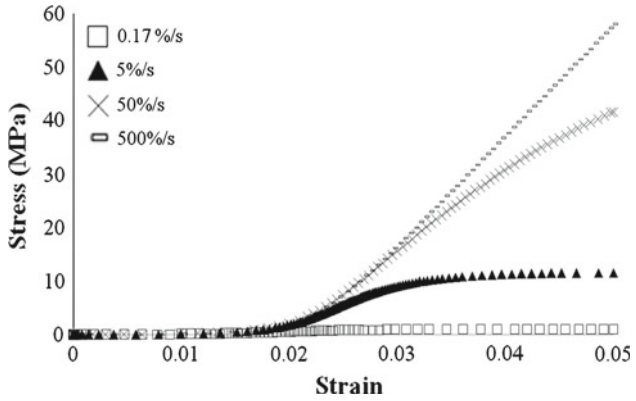

Fig. 3 Nominal stress–strain relationship of cartilage tissue at different strain rates

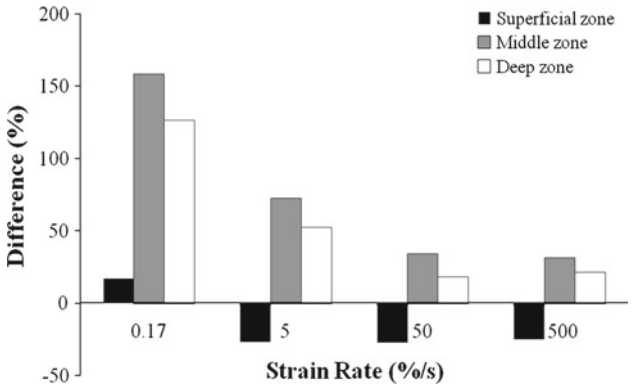

Fig. 5 Differences of peak cell strain from peak local tissue strain in the superficial, middle and deep zones subjected to four different strain rates

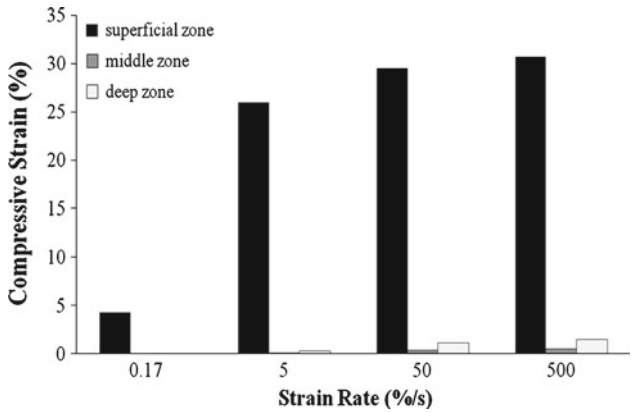

Fig. 4 Peak compressive strain of local tissue subjected to loading at four different strain rates

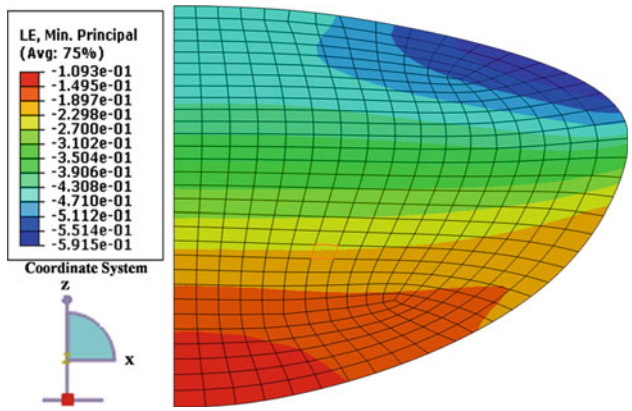

Fig. 6 Example of minimum principal strain distribution in superficial zone cell model under 5% nominal tissue strain at 500%/s

articular surface, to allow free fluid flow through the surface. Cells were studied at three locations: the superficial zone ($\xi = 0.9$), middle zone ($\xi = 0.5$) and the deep zone ($\xi = 0.1$). The time-varying solid displacements and fluid pressures at each node of the macro-scale model were used as boundary conditions for the micro-scale model.

3 Results

Changes in nominal stress–strain curve for cartilage tissue were compared for different strain rates (Fig. 3). The stress–strain curves of the cartilage tissue were all non-linear and showed increasing stiffness with increasing strain rates. The peak local compressive strain of the tissue also increased with increasing strain rates and was highest at the highest strain rate (Fig. 4). The tissue strain was amplified in the middle/deep zone cells, but attenuated in the superficial zone cells (Fig. 5).

Changes in fluid velocities through cells, cell height, hydrostatic pressure, cell membrane tangential strain and strain rates were compared for the different strain rates for the cells located in the superficial, middle and deep zone (Figs. 8, 9, 10, 11, 12). The transient responses of the cells to the mechanical loading were measured from the moment the tissue model was strained until the peak of the applied strain.

An example of strain distribution in the cells during tissue compression is shown in Fig. 6. The location of the peak tangential tensile membrane strain in the cell membrane is also given in Fig. 7.

At the highest tested strain rate (500%/s), the fluid velocity through cell was fastest, but was only 68% faster than fluid velocity at physiological strain rate (5%/s) (Fig. 8).

The cell compressive strain (Fig. 9) was also maximal at the highest strain rate (500%/s) and was smallest when loaded at the lowest loading rate (0.167%/s). However, the maximum strain at impact loading (500%/s) was only approximately 20% higher than that observed at a more physiological loading rate (5%/s).

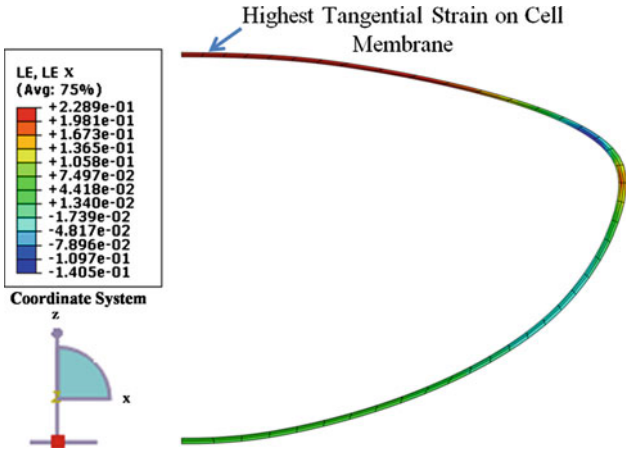

Fig. 7 Example of tangential tensile membrane strain of superficial zone cell. It was found that maximum tangential tensile strains occur at the top of the cell membrane

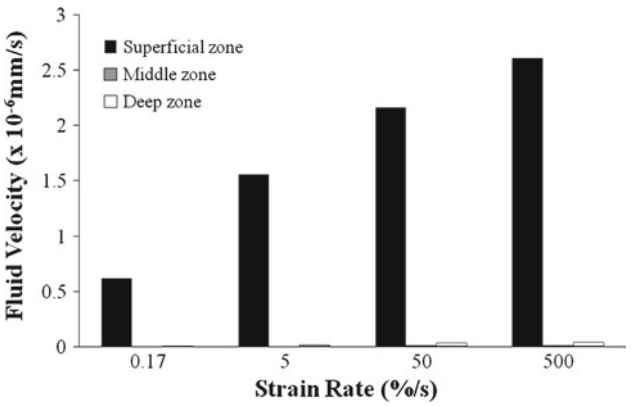

Fig. 8 Peak fluid velocities through the cell membrane for cells in the superficial, middle and deep zones of the cartilage tissue exposed to four different strain rates

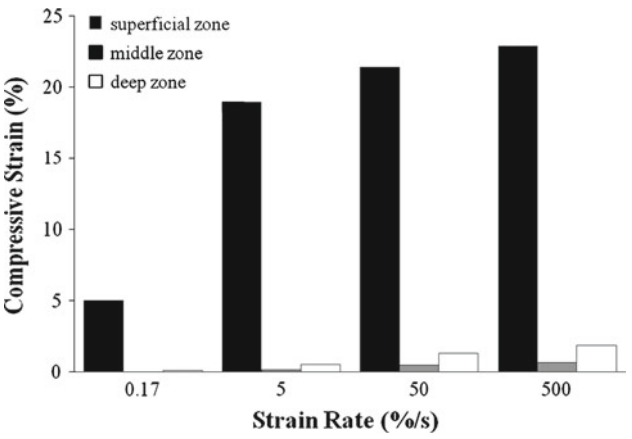

Fig. 9 Peak compressive cell strain for cells located in the superficial, middle and deep zones subjected to loading at four different strain rates

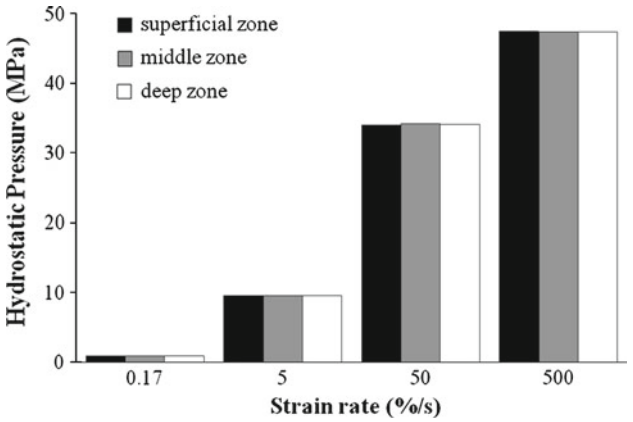

Fig. 10 Changes in peak cell pressure for cells located in the superficial, middle and deep zones subjected to loading at four different strain rates

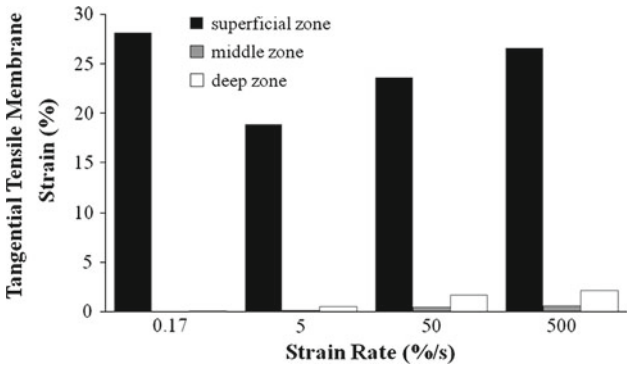

Fig. 11 Peak tangential tensile membrane strains for cells located in the superficial, middle and deep zones subjected to loading at four different strain rates

Generally, cell strains in the superficial zone were higher than those obtained in the middle/deep zone. The cell pressure (Fig. 10) increased about 50 times when loading rates increased from 0.167 to 500%/s.

The tangential tensile membrane strains in superficial zone cells (19–28%) were generally much higher than those observed in the middle/deep zone (Fig. 11). Cell membrane strains were similar across strain rates. The rate of change in tangential tensile membrane strains (Fig. 12) was highest at the highest strain rate and for the superficial zone cells.

4 Discussion

A 5% nominal strain, confined compression test was used to study why articular cartilage may die when exposed to impact loading but survive when exposed to slow loading rates of similar magnitude. Previous studies suggest that low-impact energies are sufficient to cause significant cell death without compromising the structural integrity of the extracellular matrix (Duda et al. 2001). Therefore, the strain magnitude in

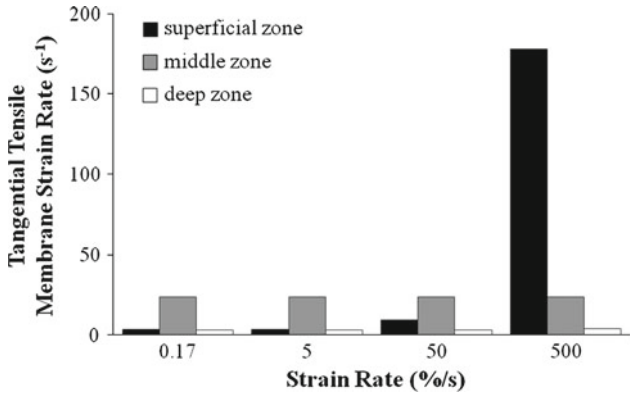

Fig. 12 Peak tangential tensile membrane strain rates for cells in the superficial, middle and deep zones of the cartilage tissue exposed to loading at four different strain rates

this study was chosen to be small so that the matrix would likely remain intact (Milentijevic et al. 2003).

Milentijevic and Torzilli (2005) quantified the effects of stress rate on in-situ chondrocyte viability. They found that when a 30 MPa stress was applied over 30 ms (stress rate of 1,000 MPa/s), a maximum nominal strain of 13.8% was measured giving an average strain rate of about 460%/s, and this led to observable cell death in the superficial zone. The cartilage tissue in our Finite Element (FE) model was subjected to a strain rate of 500 %/s. From the stress–strain relationship of the cartilage tissue (Fig. 3), this results in a stress of about 58 MPa (at a rate of 5,800 MPa/s) onto the tissue. However, there are no reports of impact loading of cartilage for a 5% strain, and thus direct comparison of our results with exactly equivalent results is not possible. Isaac et al. (2008) impacted patellae of rabbits with a load of about 45 MPa and found that the highest cell death occurred in the superficial zone. The high stress applied to the cartilage tissue could also be a factor in chondrocyte death. In our model, the stress applied at impact was 58 MPa. Therefore, it is reasonable to assume that 500%/s would lead to cell death in the superficial zone.

In the current study, the intrinsic viscoelasticity of the tissue and the cells was neglected. Therefore, the only viscoelastic effect that was taken into account is due to the biphasic nature of both tissue and cells. This choice was dictated by the fact that the viscoelasticity due to the drag force exchanged between solid and fluid phases is thought to dominate the intrinsic viscoelasticity of the solid phase (Mow et al. 1980). The stress–strain curves of the tissue model (Fig. 3) used here were shown to become steeper when the strain rates increase, which is the effect of tissue's viscoelasticity due to its biphasic nature.

The cartilage tissue (macro-scale model) was modelled assuming a homogeneous mixture of proteoglycan matrix and collagen fibres. It is known that collagen fibre orientation varies with tissue depth (Hedlund et al. 1993). Generally, collagen fibres are parallel to the articular surface in the superficial zone, randomly arranged in the middle zone and perpendicular to the tidemark in the deep zone (Hedlund et al. 1993). Since collagen fibres function predominantly in tension, and the radial stretch of the cartilage tissue in confined compression is close to zero (Li et al. 2005), and mathematically zero for a model that is homogeneous in the radial direction, it is reasonable to assume that the homogenization of proteoglycan and collagen fibres does not affect the mechanical response of the cartilage tissue significantly.

Also, the cylindrical ECM used in the micro-scale model was built according to the aspect ratio and volumetric fraction of the embedded chondrocytes at the varying tissue depths. This is a crucial step to ensure that each micro-scale model consists of only one chondron.

From the simulations' results, we found that the tissue strains were amplified at the cell level (positive values in difference) in the middle/deep zone of the tissue. Since the cells are about three orders of magnitude softer than the tissue (in the middle zone, the Young's modulus of the tissue is 700 times larger than that of the cell, whereas in deep zone, it is 1,800 times larger), cells could reasonably be treated as voids in the tissue and they would be compressed more than the local tissue. According to Chahine et al. (2007), who loaded the cartilage at a slow loading rate (0.14%/s), local tissue strains in the middle/deep zones are greatly amplified, which agrees with our findings.

In contrast, cell strains in the superficial zone were about 27% smaller than tissue strains. The difference in material strength between cells and tissue in this region is much smaller than in the middle/deep zone (in the superficial zone, the Young's modulus of the tissue is 140 times larger than that of the cell). Also, in contrast to cells in the middle/deep zone, cells in the superficial zone are flat and stiffer (refer to Table 2) (Shieh and Athanasiou 2006), which is arguably a way to protect them from large compressive deformations. All these factors contribute to the smaller cell strain compared to tissue strain in the superficial zone.

However, our simulation results suggest that superficial cells are more susceptible to changes in strain rates than cells in the middle and deep zones. The maximum compressive cell strain and the tangential membrane strain reached values of up to approximately 23% in superficial zone chondrocytes, while the applied nominal strain was merely 5%. These disparities in the magnitude of applied tissue strain with resulting cell strains were expected considering that the local tissue strains were not controlled and varied substantially because of the variable, depth-dependent material properties. The factor affecting cell mechanics the most is the local tissue strain, and a local tissue strain of 30% is reasonable for a 5% nominal tissue strain given the depth-dependent material properties of the tissue.

Compressive cell strains were highest for the highest (impact) strain rate (Fig. 9). This is to be expected, considering that the cell is three orders of magnitude softer than the surrounding ECM. For increasing rates of tissue loading, the drag forces applied increase too, as they are proportional to the filtration velocity of the fluid with respect to the solid, that is, (Hassanizadeh 1986; Grillo et al. 2009),

$$\mathrm{div}\boldsymbol{\sigma}_s = -\phi_f k^{-1}\boldsymbol{w} + p\,\mathrm{grad}\phi_f \tag{17}$$

where $\boldsymbol{\sigma}_s$ is the Cauchy stress in the solid, ϕ_f is the fluid volumetric fraction, k is the permeability, $\boldsymbol{w} = \phi_f(\boldsymbol{v}_f - \boldsymbol{v}_s)$ is the filtration velocity (given by the velocity of the fluid relative to the solid and rescaled by the fluid volumetric fraction), and p is the pore pressure. Therefore, the increasing drag forces lead to increasing stresses and thus to the increasing strain found in the local tissue. Since the cellular responses (cells are also biphasic) depend greatly on the cells' microenvironment, cell strains also increase with increasing strain rates.

Nevertheless, cell compressive strains did not reach levels where chondrocytes would be expected to die. Guilak et al. (1995) reported that in-situ cells remained alive under compressive strain as high as 30%. Also, Nguyen et al. (2009) found that mean normal cell strains of 78% were required to kill chondrocytes. Such values were not even close to those found in our computational loading protocols (the largest compressive cell strains were approximately 23% at a loading rate of 500%/s). However, previous studies have shown that compressive strains of 5% at impact rate can cause chondrocyte death in the superficial zone (Milentijevic et al. 2003; Milentijevic and Torzilli 2005). Therefore, it seems unlikely that compressive strains can kill chondrocytes during impact loading involving small tissue deformations.

Furthermore, we found that the deep zone cells strain more than middle zone cells. Similar observations were also made for local tissue strains (Fig. 4). The reason for these results might be associated with the tissue fluid flow. Although the middle zone is the most permeable to fluid flow, it experiences very small fluid flow during tissue compression, as flow is severely restricted by the superficial and deep zones. Since fluid is assumed to be incompressible, it resists compression of the cartilage. In contrast, the deep zone tissue allows a small amount of fluid to escape through the tidemark (the permeability of cartilage at the tidemark interface is $1.39 \times 10^{-16}\mathrm{m}^4/\mathrm{Ns}$, while the permeability of the bone is constant at $1.00 \times 10^{-20}\mathrm{m}^4/\mathrm{Ns}$). Even though the fluid flow through the tidemark is negligible compared to fluid flow through the articular surface, the slight difference in fluid flow between deep zone and middle zone could eventually cause the fluid resistance to compression to be smaller in the deep than the middle zone cartilage. This would lead to higher local tissue strains in the deep compared to the middle zone, which in turn leads to greater compressive and tangential strains in the deep compared to the middle zone cells.

Isolated chondrocytes have been shown to die by apoptosis when exposed to hydrostatic pressures as low as 5–10 MPa (Islam et al. 2002; Nakamura et al. 2006). However, chondrocytes protected by the PCM can resist pressures as high as 50 MPa without any apparent side effect (Nakamura et al. 2006). The highest hydrostatic pressures produced in our study occurred at the fastest (impact) strain rate and reached approximately 47 MPa (Fig. 10). This result suggests that chondrocytes would likely not have been killed in our impact loading scenario by excessive hydrostatic pressures.

We also looked into the role played by fluid velocities. Regarding the possible cause of cell necrosis, we think that the fluid velocity into/out of the cells through the cell membranes is a more important factor than fluid velocities through ECM and cell. Fluid flow would be expected to exert drag forces on the solid phase and intracellular structures, and increasing velocities would lead to greater drag forces (see Eq. (17)), which may eventually lead to damage of intracellular components. This series of events would be expected to cause cell death by apoptosis. Here, we were interested in cell necrosis associated with damage to the cell membranes and thus investigated fluid flow across the cell membranes. We found that fluid velocity across cell membranes is higher for cells in the superficial zone (Fig. 8) compared to cells in the middle/deep zones, but fluid velocity only increased by 68% for an increase in strain rates of 10,000%. Therefore, we believe that fluid velocity across cell membranes is not a significant factor in chondrocyte death during impact loading.

The greatest membrane tangential strain rates were observed at the highest strain rates and for the superficial zone cells (Fig. 12). This observation is of interest as experimental studies show that cell death due to impact loading occurs primarily in superficial zone cells (Milentijevic et al. 2003; Milentijevic and Torzilli 2005). Therefore, we suggest that the tangential membrane strain rate may play an important role in chondrocyte death associated with impact loading.

It should be mentioned that the focus of this study was to investigate the factors that cause cell necrosis, rather than apoptosis, under impact loading conditions. In most studies (Milentijevic et al. 2003; Milentijevic and Torzilli 2005; Ewers et al. 2001), cell death after impact loading occurs "instantaneously" suggesting it is a primarily necrotic event. Live cell membranes are impermeable to the probes (e.g. propidium iodide, ethidium homodimer) used to study cell death, which could only give off fluorescence when reaching the cell nucleus. Therefore, experimentally observed cell death is associated with membrane failure (Bevensee et al. 1995).

The plasma membrane is composed of a phospholipid bilayer that contains various protein subunits and glycoproteins. Various forces (van der Waal, electrostatic, hydrogen bonds and non-covalent interactions) contribute to the formation of the phospholipid bilayers. Jay and Canham (1977) studied cell membranes and found them to be viscoelastic, and failure strains have been shown to be around 2–3% (equivalent to a critical tension of about 0.5 Pa Raucher and Sheetz 1999; Sheetz and Dai 1996). A live cell, however, can buffer membrane strains with its invaginations as well as projections (Raucher and Sheetz 1999; Escolar et al. 1989; Nielsen et al. 1993). Therefore, live cell membranes can accommodate much greater strains than the failure strains obtained using isolated membrane failure experiments (Evans and Skalak 1979; Waugh 1983). Our simulation results showed large membrane tensile strains (about 30%) for all loading rates. However, since chondrocytes are known to survive 5% nominal tissue strains when these are applied slowly, these membrane strains are likely not the cause of cell death observed in impact situations with small tissue deformations.

Previous experimental results indicate that cell membrane damage is sensitive to the applied strain rate (Geddes et al. 2003; Shi and Whitebone 2006). Shi and Whitebone (2006) found that cell membrane damage was much more severe when strains were applied rapidly (355–519 s^{-1}) rather than slowly (0.006–0.008 s^{-1}). They also demonstrated that strain rate is much more important than strain magnitude by showing that a strain of 100% applied slowly caused less structural and functional damage to cell membranes than a strain of 25% applied at impact rate (Shi and Whitebone 2006).

Cells are able to repair membrane lesions through tension-reduction and patching mechanisms (McNeil and Steinhardt 2003). Therefore, cells may survive membrane damage if lesions are not big enough (Stroetz et al. 2001). However, Shi and Whitebone (2006) pointed out that the repair of membrane lesions caused by impact was incomplete, implying that the damage imparted to cell membranes during impact loading was permanent and typically led to cell necrosis.

Based on our theoretical considerations and previously published experimental results, we propose that chondrocyte death during impact loading occurs when the plasma membrane tangential strain rate exceeds a certain threshold value. Though cells can attenuate membrane strains through unfolding mechanisms, rapidly applied strains may not allow for these unfolding events to occur, causing high tensile membrane stresses and membrane failure (Nguyen et al. 2009). Using the same argument, the viability of cells in the middle/deep zones following impact loading could be explained by the fact that the cells' tangential tensile membrane strain rate is relatively smaller.

We made a series of assumptions in this study, and they must be considered when interpreting our results. First, the maximum tangential membrane strains were assumed to occur at the top, or lateral, or bottom surfaces, and were only quantified at these locations. Second, the cell and matrix were assumed to be perfectly bonded, whereas, in reality, cells are anchored to the extracellular matrix through focal adhesions (Hynes 1992). Third, cell membranes were assumed to be continuous with smooth surfaces, while in reality, they are made of phospholipid bilayers with variable surface topology. Finally, the thickness of the cell membranes was taken as 0.1 μm for numerical stability (Ateshian et al. 2007).

Despite these limitations, the current model provides insight into the chondrocyte mechanics during the transient phase of impact loading, which cannot be measured experimentally at this time. Future improvements of this model may include focal contacts between chondrocyte and extracellular matrix (Ward and Hammer 1993), a more realistic representation of cell membranes and incorporation of a cytoskeletal micro-structure (Ward and Hammer 1993). Most importantly, however, we are working to develop the experimental techniques to observe chondrocyte mechanics during impact loading in the intact joint, so that experimental validation of these findings will be possible. Good progress towards this goal has been made recently with a first ever description of chondrocyte mechanics in the intact joint loaded by muscular contractions (Abusara et al. 2011).

Acknowledgments The authors would like to thank Mr. Vincent Murphy for his advice throughout this research. Many thanks also to Mr. Jan Pajerski and Dr. Amr Guaily for their help in the numerical implementation of the simulation model, and to Dr. Marcelo Epstein for useful discussions about the theoretical part of the work. This study was supported by grants from the CIHR, the Canada Research Chair Programme, the AHFMR Team Grant on Osteoarthritis, Malaysia UM/MOHE HIR grant, Postgraduate Research Grant (grant no PS108/2010A) from IPPP, the NSERC Discovery Programme (NSERC, Canada), and the New Faculty Programme (Alberta Innovates Technology Futures, Canada).

References

Abusara Z, Seerattan R, Leumann A, Thompson R, Herzog W (2011) A novel method for determining articular cartilage chondrocyte mechanics in vivo. J Biomech 44(5):930–934

Alexopoulos LG, Setton LA, Guilak F (2005) The biomechanical role of the chondrocyte pericellular matrix in articular cartilage. Acta Biomater 1(3):317–325

Alexopoulos LG, Williams GM, Upton ML, Setton LA, Guilak F (2005) Osteoarthritic changes in the biphasic mechanical properties of the chondrocyte pericellular matrix in articular cartilage. J Biomech 38(3):509–517

Ateshian GA, Costa KD, Hung CT (2007) A theoretical analysis of water transport through chondrocytes. Biomech Model Mechanobiol 6(1–2):91–101

Bevensee MO, Schwiening CJ, Boron WF (1995) Use of bcecf and propidium iodide to assess membrane integrity of acutely isolated ca1 neurons from rat hippocampus. J Neurosci Methods 58(1–2):61–75

Blanco FJ, Guitian R, Vázquez-Martul E, de Toro FJ, Galdo F (1998) Osteoarthritis chondrocytes die by apoptosis. A possible pathway for osteoarthritis pathology. Arthr Rheum 41(2):284–289

Brandt K, Mankin H, Shulman L (1986) Workshop on etiopathogenesis of osteoarthritis. J Rheumatol 13:1126–1160

Chahine NO, Ateshian GA, Hung CT (2007) The effect of finite compressive strain on chondrocyte viability in statically loaded bovine articular cartilage. Biomech Model Mechanobiol 6(1–2):103–111

Duda GN, Eilers M, Loh L, Hoffman JE, K*ää*b M, Schaser K (2001) Chondrocyte death precedes structural damage in blunt impact trauma. Clin Orthop Relat Res 393:302–309

Escolar G, Leistikow E, White JG (1989) The fate of the open canalicular system in surface and suspension-activated platelets. Blood 74(6):1983–1988

Evans EA, Skalak R (1979) Mechanics and thermodynamics of biomembranes: part 1. CRC Crit Rev Bioeng 3(3):181–330

Ewers BJ, Dvoracek-Driksna D, Orth MW, Haut RC (2001) The extent of matrix damage and chondrocyte death in mechanically traumatized articular cartilage explants depends on rate of loading. J Orthop Res Off Publ Orthop Res Soc 19(5):779–784

Federico S, Grillo A, Herzog W (2004) A transversely isotropic composite with a statistical distribution of spheroidal inclusions: a geometrical approach to overall properties. J Mech Phys Solids 52(10):2309–2327

Federico S, Grillo A, Larosa G, Giaquinta G, Herzog W (2005) A transversely isotropic, transversely homogeneous microstructural-statistical model of articular cartilage. Jv Biomech 38(10):2008–2018

Geddes DM, Cargill RS, LaPlaca MC (2003) Mechanical stretch to neurons results in a strain rate and magnitude-dependent increase in plasma membrane permeability. J Neurotrauma 20(10):1039–1049

Grillo A, Wittum G, Giaquinta G, Micunovic MV (2009) A multiscale analysis of growth and diffusion dynamics in biological materials. Int J Eng Sci 47(2):261–283

Guilak F, Mow VC (1992) Determination of the mechanical response of the chondrocyte in situ using finite element modeling and confocal microscopy. ASME Adv Bioeng BED 20:21–23

Guilak F, Mow VC (2000) The mechanical environment of the chondrocyte: a biphasic finite element model of cell-matrix interactions in articular cartilage. J Biomech 33(12):1663–1673

Guilak F, Ratcliffe A, Mow VC (1995) Chondrocyte deformation and local tissue strain in articular cartilage: a confocal microscopy study. J Orthop Res Off Publ Orthop Res Soc 13(3):410–421

Han SK, Federico S, Grillo A, Giaquinta G, Herzog W (2007) The mechanical behaviour of chondrocytes predicted with a microstructural model of articular cartilage. Biomech Model Mechanobiol 6(3):139–150

Han SK, Federico S, Herzog W (2011) A depth-dependent model of the pericellular microenvironment of chondrocytes in articular cartilage. Comput Methods Biomech Biomed Eng 14(7):657–664

Hassanizadeh SM (1986) Derivation of basic equations of mass transport in porous media, part 1. Macroscopic balance laws. Adv Water Resour 9(4):196–206

Hedlund H, Mengarelli-Widholm S, Reinholt FP, Svensson O (1993) Stereologic studies on collagen in bovine articular cartilage. APMIS 101(1–6):133–140

Holmes MH, Mow VC (1990) The nonlinear characteristics of soft gels and hydrated connective tissues in ultrafiltration. J Biomech 23(11):1145–1156

Hynes RO (1992) Integrins: versatility, modulation, and signaling in cell adhesion. Cell 69(1):11–25

Isaac DI, Meyer EG, Haut RC (2008) Chondrocyte damage and contact pressures following impact on the rabbit tibiofemoral joint. J Biomech Eng 130(4):041,018–041,018

Islam N, Haqqi TM, Jepsen KJ, Kraay M, Welter JF, Goldberg VM, Malemud CJ (2002) Hydrostatic pressure induces apoptosis in human chondrocytes from osteoarthritic cartilage through up-regulation of tumor necrosis factor-alpha, inducible nitric oxide synthase, p53, c-myc, and bax-alpha, and suppression of bcl-2. J Cell Biochem 87(3):266–278

Jay AW, Canham PB (1977) Viscoelastic properties of the human red blood cell membrane. ii. area and volume of individual red cells entering a micropipette. Biophys J 17(2):169–178

Kurz B, Jin M, Patwari P, Cheng DM, Lark MW, Grodzinsky AJ (2001) Biosynthetic response and mechanical properties of articular cartilage after injurious compression. J Orthop Res 19(6):1140–1146

Li L, Herzog W, Korhonen R, Jurvelin J (2005) The role of viscoelasticity of collagen fibers in articular cartilage: axial tension versus compression. Med Eng Phys 27(1):51–57

Mankin HJ (1963) Localization of tritiated thymidine in articular cartilage of rabbits: Iii. Mature articular cartilage. J Bone Jt Surg Am 45(3):529–540

Maroudas A, Bullough P (1968) Permeability of articular cartilage. Nature 219(5160):1260–1261

McNeil PL, Steinhardt RA (2003) Plasma membrane disruption: repair, prevention, adaptation. Annu Rev Cell Dev Biol 19:697–731

Milentijevic D, Torzilli PA (2005) Influence of stress rate on water loss, matrix deformation and chondrocyte viability in impacted articular cartilage. J Biomech 38(3):493–502

Milentijevic D, Helfet DL, Torzilli PA (2003) Influence of stress magnitude on water loss and chondrocyte viability in impacted articular cartilage. J Biomech Eng 125(5):594–601

Mow VC, Guilak F (1993) Deformation of chondrocytes within the extracellular matrix of articular cartilage. Birkh*ä*user, Boston 128–145

Mow VC, Kuei SC, Lai WM, Armstrong CG (1980) Biphasic creep and stress relaxation of articular cartilage in compression: theory and experiments. J Biomech Eng 102(1):73–84

Nakamura S, Arai Y, Takahashi KA, Terauchi R, Ohashi S, Mazda O, Imanishi J, Inoue A, Tonomura H, Kubo T (2006) Hydrostatic pressure induces apoptosis of chondrocytes cultured in alginate beads. J Orthop Res Off Publ Orthop Res Soc 24(4):733–739

Nguyen BV, Wang Q, Kuiper NJ, El Haj AJ, Thomas CR, Zhang Z (2009) Strain-dependent viscoelastic behaviour and rupture force of single chondrocytes and chondrons under compression. Biotechnol Lett 31(6):803–809

Nielsen S, DiGiovanni SR, Christensen EI, Knepper MA, Harris HW (1993) Cellular and subcellular immunolocalization of vasopressin-regulated water channel in rat kidney. Proc Natl Acad Sci USA 90(24):11,663–11,667

Poole CA, Flint MH, Beaumont BW (1987) Chondrons in cartilage: ultrastructural analysis of the pericellular microenvironment in adult human articular cartilages. J Orthop Res Off Publ Orthop Res Soc 5(4):509–522

Quinn TM, Allen RG, Schalet BJ, Perumbuli P, Hunziker EB (2001) Matrix and cell injury due to sub-impact loading of adult bovine articular cartilage explants: effects of strain rate and peak stress. J Orthop Res Off Publ Orthop Res Soc 19(2):242–249

Raucher D, Sheetz MP (1999) Characteristics of a membrane reservoir buffering membrane tension. Biophys J 77(4):1992–2002

Repo RU, Finlay JB (1977) Survival of articular cartilage after controlled impact. J Bone Jt Surg A 59(8):1068–1076

Schinagl RM, Gurskis D, Chen AC, Sah RL (1997) Depth-dependent confined compression modulus of full-thickness bovine articular cartilage. J Orthop Res Off Publ Orthop Res Soc 15(4):499–506

Sheetz MP, Dai J (1996) Modulation of membrane dynamics and cell motility by membrane tension. Trends Cell Biol 6(3):85–89

Shi R, Whitebone J (2006) Conduction deficits and membrane disruption of spinal cord axons as a function of magnitude and rate of strain. J Neurophysiol 95(6):3384–3390

Shieh AC, Athanasiou KA (2006) Biomechanics of single zonal chondrocytes. J Biomech 39(9):1595–1602

Simon WH, Richardson S, Herman W, Parsons JR, Lane J (1976) Long-term effects of chondrocyte death on rabbit articular cartilage in vivo. J Bone Jt Surg Am 58(4):517–526

Stroetz RW, Vlahakis NE, Walters BJ, Schroeder MA, Hubmayr RD (2001) Validation of a new live cell strain system: characterization of plasma membrane stress failure. J Appl Physiol 90(6):2361–2370

Trickey WR, Lee GM, Guilak F (2000) Viscoelastic properties of chondrocytes from normal and osteoarthritic human cartilage. J Orthop Res Off Publ Orthop Res Soc 18(6):891–898

Wang CCB, Chahine NO, Hung CT, Ateshian GA (2003) Optical determination of anisotropic material properties of bovine articular cartilage in compression. J Biomech 36(3):339–353

Ward MD, Hammer DA (1993) A theoretical analysis for the effect of focal contact formation on cell-substrate attachment strength. Biophys J 64(3):936–959

Waugh RE (1983) Effects of abnormal cytoskeletal structure on erythrocyte membrane mechanical properties. Cell Motil 3(5–6):609–622

Wu JZ, Herzog W (2000) Finite element simulation of location- and time-dependent mechanical behavior of chondrocytes in unconfined compression tests. Ann Biomed Eng 28(3):318–330